Tertiary block rotations in the Fars Arc (Zagros, Iran)

Charles Aubourg, Brigitte Smith, H. R. Bakhtari, N. Guya, A. Eshraghi

Geophys. J. Int. (2008) **173,** 659–673 doi: 10.1111/j.1365-246X.2008.03732.x

Tertiary block rotations in the Fars Arc (Zagros, Iran)

C. Aubourg,[1] B. Smith,[2] H. R. Bakhtari,[3] N. Guya[3] and A. Eshraghi[4]

[1] *Laboratoire de Tectonique, Université Cergy Pontoise, CNRS.* 5*, mail Gay Lussac. Neuville-sur-Oise,* 95031 *Cergy, France. E-mail: aubourg@u-cergy.fr*
[2] *Géosciences Montpellier, Université de Montpellier* 2*, CNRS, Place Eugène Bataillon,* 34095 *Montpellier, France*
[3] *Institute of Geophysics, University of Tehran, Iran*
[4] *Geological Survey of Iran, Tehran, Iran*

Accepted 2008 January 10. Received 2008 January 10; in original form 2007 May 14

SUMMARY

The Fars arc accommodates the oblique convergence between the Arabic plate and the Iran block. Many geological observations suggest block rotations from regional to local scales. We present palaeomagnetic investigations in the Fars arc and its eastern termination, the Zagros-Makran syntaxis. Sixty-four sites have been sampled covering the Palaeocene Pabdeh Fm. to Mio-Pliocene Agha-Jhari Fm., the latest being the most sampled formation. We document pre-tilting components in all formations. However, coarse fractions of Agha-Jhari clastics formation retain a post-tilting remagnetization. As a whole, block rotations rarely exceed 20°. In the western Fars arc, clockwise and counter-clockwise rotations of small amplitudes are consistent with the torsions observed near the strike slip Kazerun and Mangarak faults. In the Zagros Makran syntaxis, counter-clockwise and clockwise rotations are observed, respectively, in the western and eastern part. This pattern is consistent with an amplification of the shape of the syntaxis. Between Zagros and Makran, palaeomagnetic data support that the present-day arcuate shape of the arc is secondary. We assume that most of the block rotations took place during the Plio-Pleistocene, during a blocking stage of the Zagros-Makran syntaxis. We emphasize the role of Oman Peninsula which plays as an indenter for the propagation of the Fars thrust belt.

Key words: Palaeomagnetism applied to tectonics; Remagnetization; Folds and folding; Crustal structure; Asia.

INTRODUCTION

The Zagros Simply Folded Belt (ZSFB, Fig. 1a) accommodates one third of an oblique continental collision between Arabia and Iran block since the Miocene (Berberian 1995; Jackson *et al.* 1995; Hessami *et al.* 2001b) with evident tectonic activity nowadays (Figs 1b and c). The Fars Arc is the easternmost part of the ZSFB (Ricou *et al.* 1977). It is bounded laterally by the Kazerun fault to the west and by the Zagros-Makran Syntaxis (ZMS) to the east. The Zendan fault marks the limit between ZSFB and the Makran (Regard *et al.* 2004). Many factors suggest block rotation at different scales in Zagros. At the scale of lithospheric plate, the ∼N55° oblique convergence of Arabian plate relative to Iran block (McClay *et al.* 2004; Talebian & Jackson 2004) (Fig. 1b) can be a source of rotation. At the scale of the folded foreland of Zagros, there is a succession of syntaxis and antiaxis as illustrated easterly with the Fars Arc and the ZMS. At a large scale, this pattern can be explained by torsions of the structures, assuming that their trend was initially linear. Finally at a small scale, the frequent bended shape of folds (Ricou 1976; Bakhtari *et al.* 1998; Smith *et al.* 2005) suggests also block rotations around vertical axis.

However, very few palaeomagnetic data are available in Zagros in order to depict the block rotations. Northwest of the Zagros belt, in the Pusht-e Kuh Arc, a magnetostratigraphic study in Mio-Pliocene syn-orogenic clastics (Agha-Jahri Fm.) (Homke *et al.* 2004) indicates an absence of significant palaeomagnetic rotations in two representative folds (Fig. 1a). By contrast, the palaeomagnetic study of Smith *et al.* (2005) documents a ∼20° clockwise rotation in Agha-Jhari Fm. in the southeastern part of Zagros (Fig. 1a). In the western Makran, close to the Zendan Fault, Delaunay *et al.* (2002) report a remagnetization in Eocene flysch acquired during the latest stage of folding. This suggests that no significant rotations occurred east from Zendan fault since at least the Pleistocene.

Despite the scarce number of palaeomagnetic data, several scenarios involving block rotations have been proposed in the Fars Arc (Fig. 1a). Several studies suggested clockwise rotations in the western Fars Arc (Bakhtari *et al.* 1998; Authemayou *et al.* 2006; Lacombe *et al.* 2006), based on the shortening direction at a regional scale and the occurrence of dextral strike slip faults. Hessami *et al.* (2001a) proposed a model of block rotations within the basement of the Fars Arc. Their analysis is based on the observation of important faults and lineaments revealed by remote sensing (e.g. Furst 1990) which were initially part of the Arabian old fault network. They proposed a pattern of block rotations which is opposite to the bended shape of the Fars arc and the ZMS (Fig. 1a). Using *P*-axis pattern or earthquakes, Talebian & Jackson (2004) strengthened the

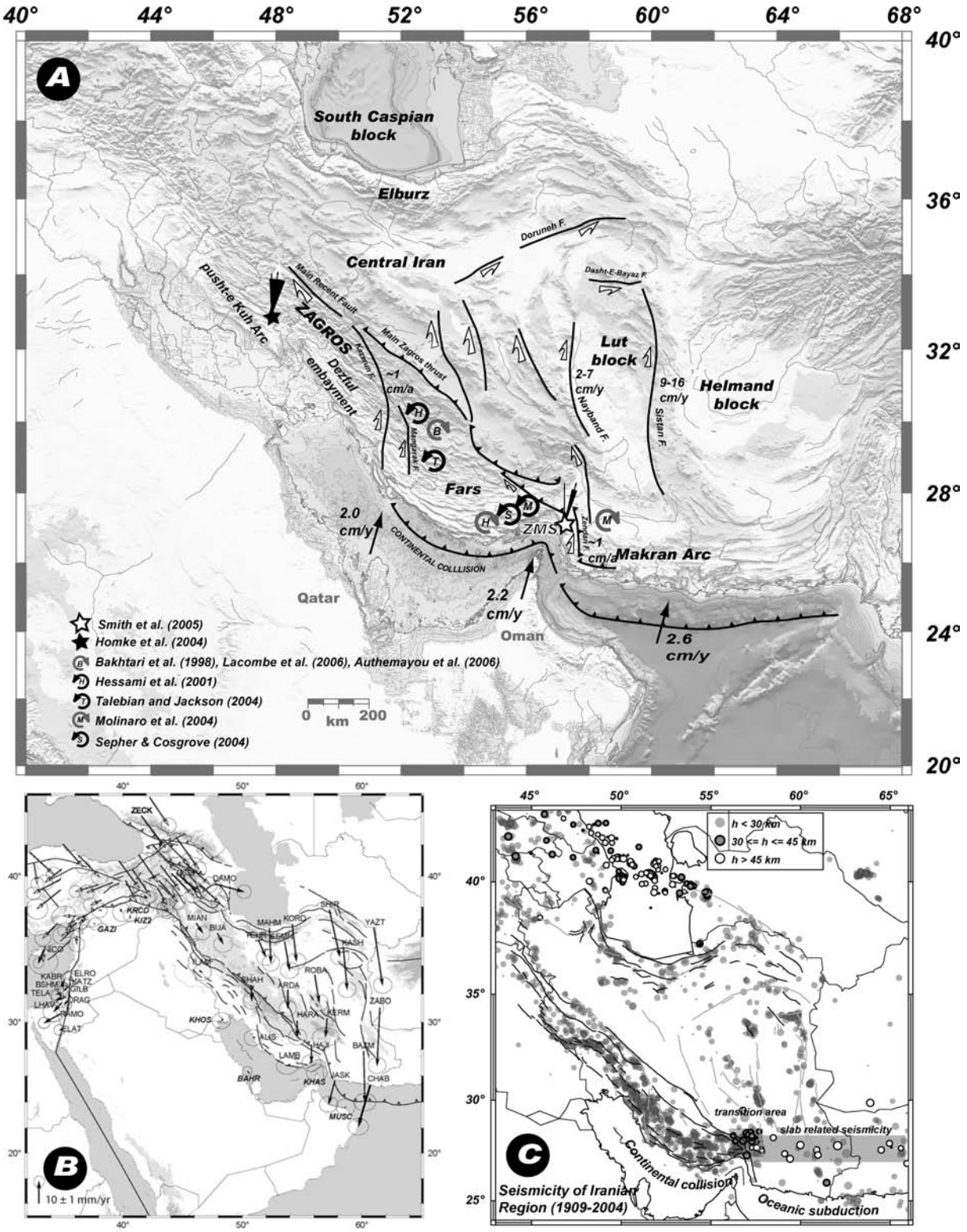

Figure 1. (a) Geodynamic framework of Zagros simply fold belt and the Zagros Makran syntaxis (labelled ZMS). The faults surrounding the Fars arc and surrounding area are indicated with their velocities and motion according to Walker *et al.* (2003). Thick arrows show GPS velocities of Arabia plate motion relative to Eurasia (Vernant *et al.* 2004). The stars indicate location of already published palaeomagnetic studies in the Agha-Jhari Fm. We show the declination of pre-tilting characteristic magnetization with its confidence angle at 95 per cent. Circular arrows correspond to sense of block rotation proposed in the literature. (b) GPS horizontal velocity and their 95 per cent confidence ellipse in Arabia fixed reference frame from 1999 to 2001 (Vernant *et al.* 2004). (c) Seismicity of Iran (1964–1998) (Engdahl & Bergman 2004).

Hessami *et al.* hypothesis and proposed also 10°–20° counter-clockwise rotation in the central Fars Arc from the last 5 Myr. Molinaro *et al.* (2004, 2005) proposed clockwise and counter-clockwise rotations in western Makran and in eastern Fars Arc, respectively, in a model of Fars and Makran arcs development. Similarly, advocating a different model, Sepehr & Cosgrove (2004) suggested substantial counter-clockwise rotations in the eastern part of Fars arc. Obviously, all these predictions of vertical axis rotations do not agree with each other.

This study aims to depict the pattern of block rotations in the Fars Arc and the ZMS by using palaeomagnetism. This work extends to the whole Fars Arc the Smith *et al.* (2005) work limited to the Minab fold. We collected and measured about 400 samples from 64 Cenozoic sites. The magnetic fabric, magnetic mineralogy, and preliminary palaeomagnetic data of these sites have been already published in Bakhtari *et al.* (1998), Delaunay *et al.* (2002), Aubourg & Robion (2002), Aubourg *et al.* (2004) and Smith *et al.* (2005).

GEOLOGICAL SETTING

Detailed information about geological setting and sampling can be found in Bakhtari *et al.* (1998) and Aubourg *et al.* (2004). The ∼12 km stratigraphic sequence of the Permian to Quaternary rocks can be summarized as follows: (1) a thick Cambrian sequence of Hormuz salt; (2) a Meso-Cenozoic carbonate shelf sequence and (3) a Neogene-Quaternary syn-orogenic clastics sequence (the Fars Group). The Hormuz salt constitutes the main detachment level of the Zagros cover in the Fars Arc (O'Brien 1957; Davis & Engelder 1985). Oblique collision between the African continental lithosphere and the Iranian block started in the Oligo-Miocene in NW Zagros and propagated to the SE (Berberian 1995). This collision is interrupted east from the Bandar-Abbas syntaxis (Fig. 1a). The Zagros belt accommodates today about one third of the ∼N10 oblique convergence (Fig. 1b), which has remained unchanged for the last 5 Myr (Talebian & Jackson 2004) or a little bit older in the Pusht-e Kuh arc (Homke *et al.* 2004).

At a regional scale, we observe from west to east; the Fars Arc, the ZMS, and the Makran Arc (Fig. 2). From NE to SW, four major faults make-up the Fars Arc; the Main Zagros Thrust Fault, the High Zagros Thrust Fault, the Mountain Front Fault and the Zagros Front Fault. The present limit of deformation is located offshore along the Persian Gulf. The Main Zagros Thrust Fault is generally considered as the suture between Iranian and Arabian plates formed during the closure of the Neo-Tethys which was initiated in the Late Cretaceous (Alavi 1994; Berberian 1995). Between the Main Zagros Thrust Fault and the High Zagros Fault, is the imbricated belt with little tectonic activity today (Fig. 1c). South of the High Zagros Fault is the Simply Folded Belt. Seismicity is confined between the Mountain Front Fault and the present-day deformation front (Fig. 1c). Balanced cross sections within the Fars Arc (Blanc *et al.* 2003; McQuarrie 2004; Molinaro *et al.* 2004; Sherkati & Letouzey 2004) suggest ∼20 per cent of shortening of the sedimentary cover since the Miocene. All cross sections emphasize the role of basement faults, possibly during the latest stages of shortening (Molinaro *et al.* 2004). Whilst the convergence direction between Arabian plate and Eurasia is relatively consistent throughout the Fars Arc and the ZMS,

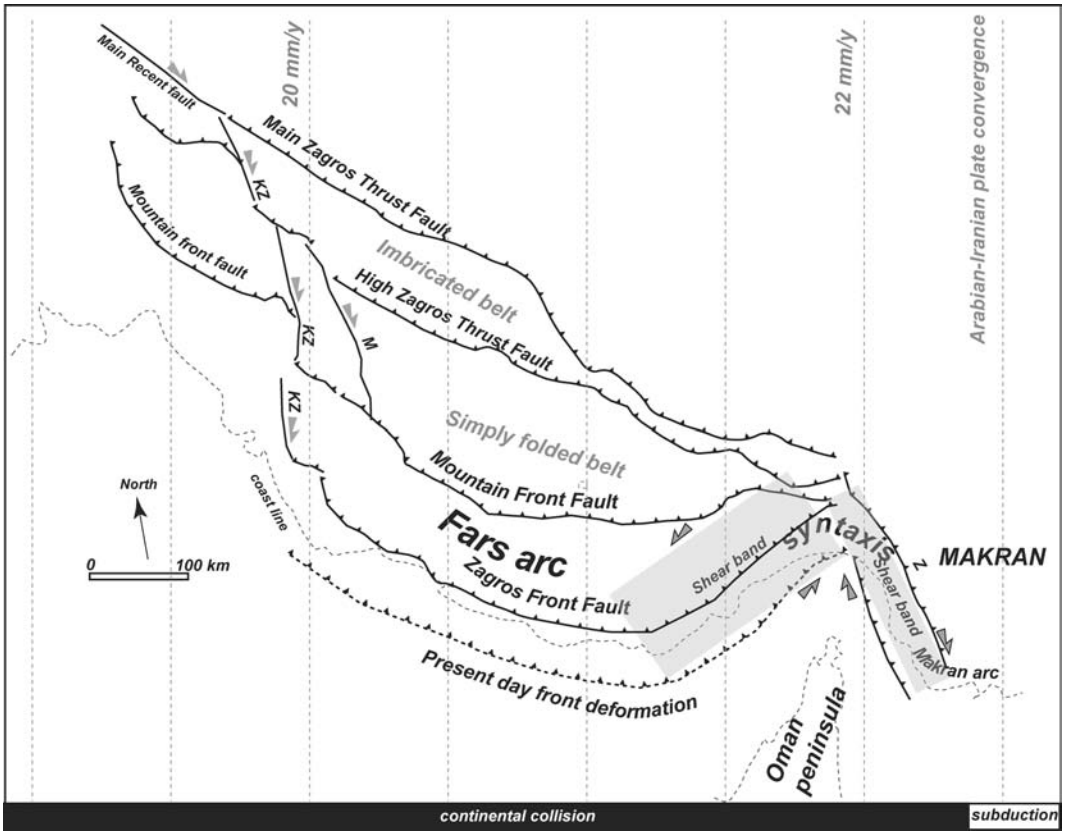

Figure 2. Sketch illustrating the major tectonic features in the Fars Arc and the eastern Makran (inspired from Sepehr & Cosgrove 2004). We plot the structures with respect to the convergence direction of Arabia relative to the Iranian plates. Note the asymmetry between the western part and eastern part of the Fars Arc. Shaded areas in the Zagros Makran Syntaxis correspond to shear zones proposed by Aubourg *et al.* (2004), in the hypothesis of the Oman peninsula acting as an indenter. KZ: Kazerun fault, M: Mangarak F., Z: Zendan F.

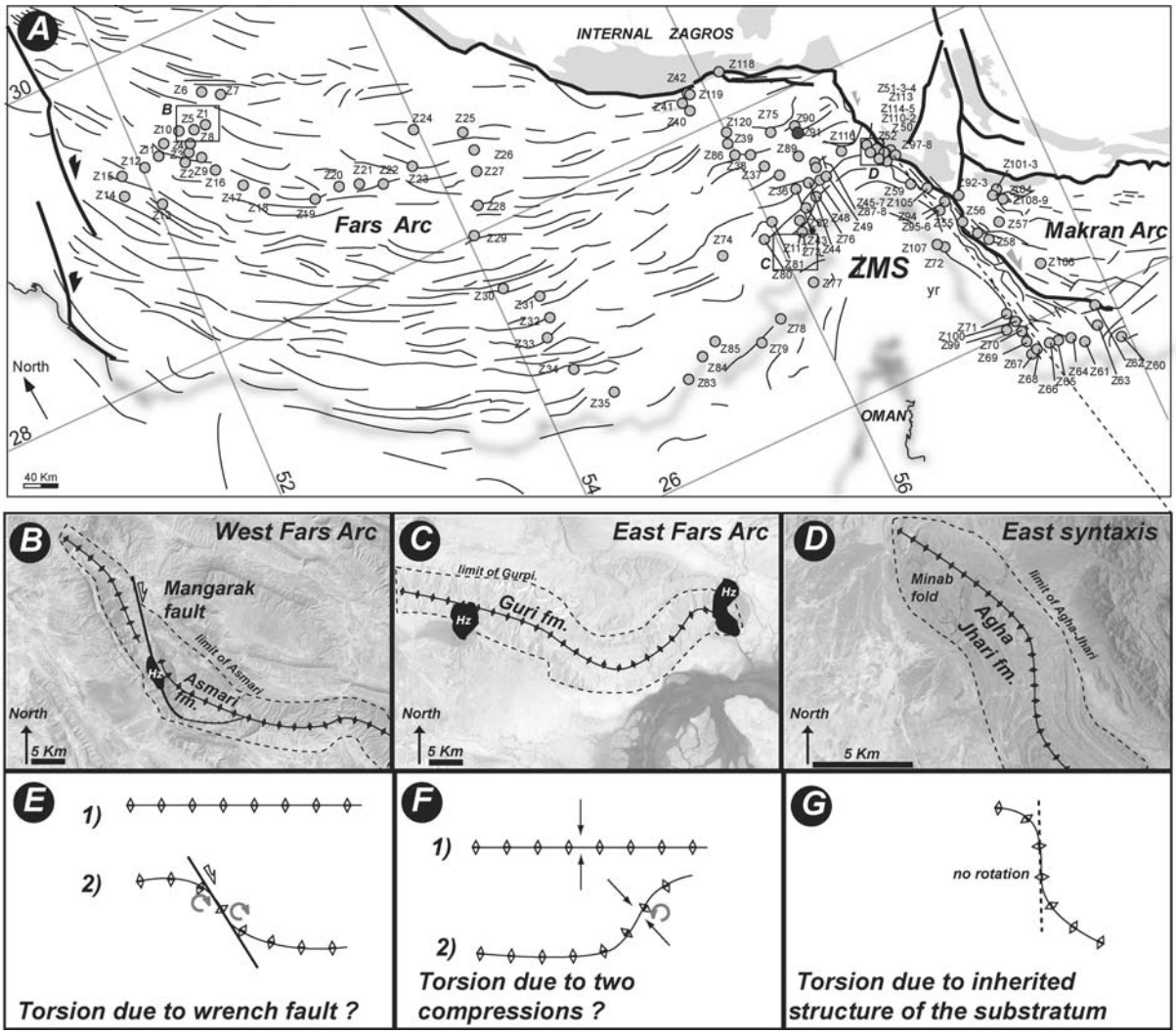

Figure 3. (a) Location of palaeomagnetic sites (circles). (b–d) Examples of bended folds (Landsat pictures). Hz is the lower Cambrian salt (Hormuz Fm.). (e–g) Different possible processes of fold torsion are sketched. Apart from the Minab fold (D) where palaeomagnetic data indicate that the curvature is primary (Smith *et al.* 2005), the torsion of the two other folds (B-C) is not yet elucidated. See text for more explanations.

the pattern of *P*-axes inferred from CMT foci, as well as shortening direction inferred from magnetic fabric, mimic the bended shape of antiaxis and syntaxis (Aubourg *et al.* 2004). Note that the Fars Arc is not symmetric (Sepehr & Cosgrove 2004). In its western part, the High Zagros Fault, the Mountain Front Fault, the Zagros Front Fault and the present-day front deformation are largely separated and linked together through the dextral still active Kazerun fault (Talebian & Jackson 2004; Authemayou *et al.* 2006). In the eastern Fars Arc, these major tectonic features almost join together. This supports the idea that the Oman Peninsula plays as an obstacle for the propagation of the fold belt (Sepehr & Cosgrove 2004). Aubourg *et al.* (2004) proposed that each side of the syntaxis is underlined by a shear band, with the development of en-échelon folds, sigmoidal folds, and a network of dextral and senestral faults.

In Zagros, the bended shape of the folds (Figs 3b–d) is a dominant feature, the interpretation of which is still subject to debate (Ricou 1976; Sattarzadeh *et al.* 2002; Aubourg *et al.* 2004; Molinaro *et al.* 2004; Authemayou *et al.* 2006). In Fig. 3, we sketch three geological processes able to generate torsion in a fold. The strike slip fault in underlying basement (Figs 3b and e) is probably the most commonly invoked process to induce a torsion in a fold, as confirmed by analogical modelling (Richard *et al.* 1991). Fold torsion is accommodated by rotation along vertical axis, and hence the bended shape of fold can help to infer the sense of strike slip motion (Fig. 3e). This characteristic was first used in the Zagros by Furst (1990) to infer the sense of a blind strike slip fault in the eastern part of the Fars Arc. We show an example of sigmoidal and disrupted fold (Fig. 3b) along the Mangarak strike slip fault. The torsion of the fold is consistent with its present-day dextral motion (Talebian & Jackson 2004; Authemayou *et al.* 2006). Another common process to account for bended shape is the succession of several non-coaxial shortening events (Fig. 3f). We show an example (Fig. 3c) of an anticline from the eastern part of the Fars Arc. There is no evident blind fault below this fold, and its bended shape can be attributed to multiple non-coaxial shortening events. If this mechanism is correct, one can expect counter-clockwise rotation of limb in this example. Ricou (1976) advocated two successive shortening events in the Fars arc in order to explain the torsions observed frequently in folds. Finally, bended fold can result from inherited structures in Mesozoic substratum (Fig. 3g) as proposed by Bakhtari *et al.* (1998). In this case, no rotation is necessary to explain the curved shape of fold. The Minab anticline is a good example (Fig. 3d) where palaeomagnetic

data demonstrated that torsion is not secondary (Smith *et al.* 2005). The torsion can be due to the draping of the fold over an inherited structure in the Mesozoic cover and from a differential deformation rate in competent and incompetent levels inside the fold. Additional mechanisms can also be invoked such as differential high-friction and low-friction of décollement levels.

SAMPLING AND ROCK MAGNETISM

We sampled Pabdeh Fm. (Palaeocene) to Agha-Jhari Fm. (Mio-Pliocene); with a main emphasis on this latter (∼70 per cent of samples). A large part of sampling was initially devoted to magnetic fabric investigation without particular focus on fold test and selection of the finest grain samples, particularly in Agha-Jhari clastic Formation. We collected samples with portable drilling machine and oriented cores using magnetic compass and sun angle. Pabdeh Fm. rocks (Palaeocene, two sites) are characterised by a succession of thin marly limestones and marls. Asmari Fm. (Eocene-Oligocene, three sites) rocks are thick shallow marine limestones. All rocks younger than Asmari Fm. belong to the Fars Group, which represents the post collision transgressive sequence of the Zagros (Sepehr & Cosgrove 2004). The Razak Fm. (Oligocene-Miocene, 11 sites) consists of red marls and clastics east from the Kazerun fault. The Guri rocks (Lower Miocene, two sites) are limestones. The Mishan Fm. (middle Miocene, one site) consists of thin bedded blue marls and the Agha-Jhari Fm. (late Miocene to Pliocene, 45 sites) of fluvial reds marls and sandstones. Homke *et al.* (2004) provided magnetostratigraphic dating of the base of Agha-Jhari at 12.8–12.3 Myr in the front al parts of the Pusht-e Kuh Arc (Lurestan stratigraphic Province). We also report palaeomagnetic result in 1 site from the Eocene Oligocene Makran flysch along the Zendan fault.

Rock magnetism of rocks from Zagros is thoroughly described in Bakhtari *et al.* (1998), Aubourg *et al.* (2004), Delaunay *et al.* (2002) and Smith *et al.* (2003). Rock magnetism analyses are based upon thermomagnetic curves (magnetic susceptibility versus temperature), three axes stepwise thermal demagnetization of isothermal remanent magnetization, hysteresis loops and thin sections analysis. In the Agha-Jahri Fm., the magnetic carriers consist essentially of coarse detrital magnetites. Subsidiary fine magnetites and pigmentary hematites carry the ChRM (Smith *et al.* 2005). It should be noted that greigite has been detected in Agha-Jahri Fm. and also within Eocene flysch from western Makran (Aubourg & Robion 2002). The Mishan Fm. shows only magnetites. The Guri Fm. displays one main ferromagnetic carrier, either magnetite or soft coercivity hematite. Razak Fm. displays often a mixture assemblage with magnetite as the most frequent mineral and hematite as accessory mineral.

PALAEOMAGNETIC RESULTS

General trends

We measured NRM using both a Squid CTF cryogenic magnetometer and a JR5 spinner magnetometer. AF demagnetization was performed using a Molspin and Agico devices, equipped with three-axes tumbler. For heating, we used a shielded furnace with ∼50 nT residual magnetic field. From pilot demagnetization, we found that thermal demagnetization was the most efficient method to clean NRM in Cenozoic rock from Zagros. AF demagnetization was efficient in five sites. We obtained frequently undesirable components at high temperatures (>400 °C) due to chemical transformation produced by the heating process. Also, a large drop of magnetization intensity is generally observed before ∼200–300 °C (Fig. 4), which makes difficult to find stable magnetization. We show typical examples of thermal demagnetization (Fig. 4). Normal and reverse polarities are observed. We processed palaeomagnetic data using Palaeomac software (Cogné 2003). We used mostly principal component analysis to determine the direction of the magnetization components. More rarely, we used great circle analysis. The synthetic results are displayed in the Table 1. The fold or tilt test helps to infer the age of a magnetization component. Unfortunately, in the present study, only few sites are suitable for a fold test, therefore, we used the expected inclination for a given age as a reference, and compare the observed declination with the expected one. If the observed inclination is consistent with the expected inclination, then the corresponding coordinate system is likely to be the correct one at the magnetization acquisition time. In the following, we call component A component of normal polarity which is close to the recent geomagnetic field in geographic coordinates ($D = 0°$; $I = 47°$ at the 28°N latitude). This component has unblocking temperatures ranging from room temperatures up to 700 °C. When unblocking temperature is lower than 300 °C, component A is likely a viscous component of the recent Earth magnetic field. Above this range of unblocking temperature, component A is likely a remagnetization. We call component B all other components in geographic coordinates away from recent geomagnetic field. Generally, a viscous component A of normal polarity accompanies the component B at low temperature ($T < 400$ °C). We do not mention this component A in our table as it is very close to present magnetic field dipole. All results are compiled in Table 1. To calculate the directions expected at each site, we used master curves of the Africa APWP since 70 Ma compiled by Besse & Courtillot (1991). Generally, the component B is not well constrained, with a scattering of directions, or a small number of samples (Table 1). The polarity is mixed, with a dominance of normal polarity. These results are similar to those reported by Homke *et al.* (2004) in the Agha-Jhari Fm . However, Smith *et al.* (2005) reported better results in Agha-Jhari Fm. when selecting the finest grained sediments. Both palaeomagnetic studies document pre-tilting, and presumably primary characteristic magnetization in the Agha-Jhari Fm.

Western Fars Arc

In the western Fars Arc, we sampled rocks from Palaeocene-Eocene (Pabdeh Fm.) to Miocene-Pliocene (Agha-Jhari Fm.). Among 28 sites, 13 sites display only the secondary component A ($D = 1°$; $I = 44°$; $\alpha_{95} = 3.1$; $K = 98$; Fig. 5a). We now examine components A and B for rocks of different ages.

The two sites of the Palaeocene-Eocene Pabdeh Fm. provide a B component (Fig. 5b). Site Z10 shows a medium temperature component of mixed polarities. According to the values of the inclination, this direction is likely post or syn-tectonic (Fig. 5b, Table 1). Site Z11 displays a good quality high temperature component of reversed polarity, up to the highest unblocking temperatures (T_{ub}) of 700 °C (Fig. 4a, Table 1), indicating, therefore, that hematite contributes to the NRM. This component is likely pre-tilting (Fig. 5b).

We studied three sites in the Eocene-Oligocene limestones of the Asmari Fm. (Table 1, Fig. 5b). The magnetization is weak and often noisy. All components have normal polarity. Sites Z2 and Z4 exhibit only component A. Site Z3 displays ill-defined component B deviated to the NW quadrant in geographic coordinates.

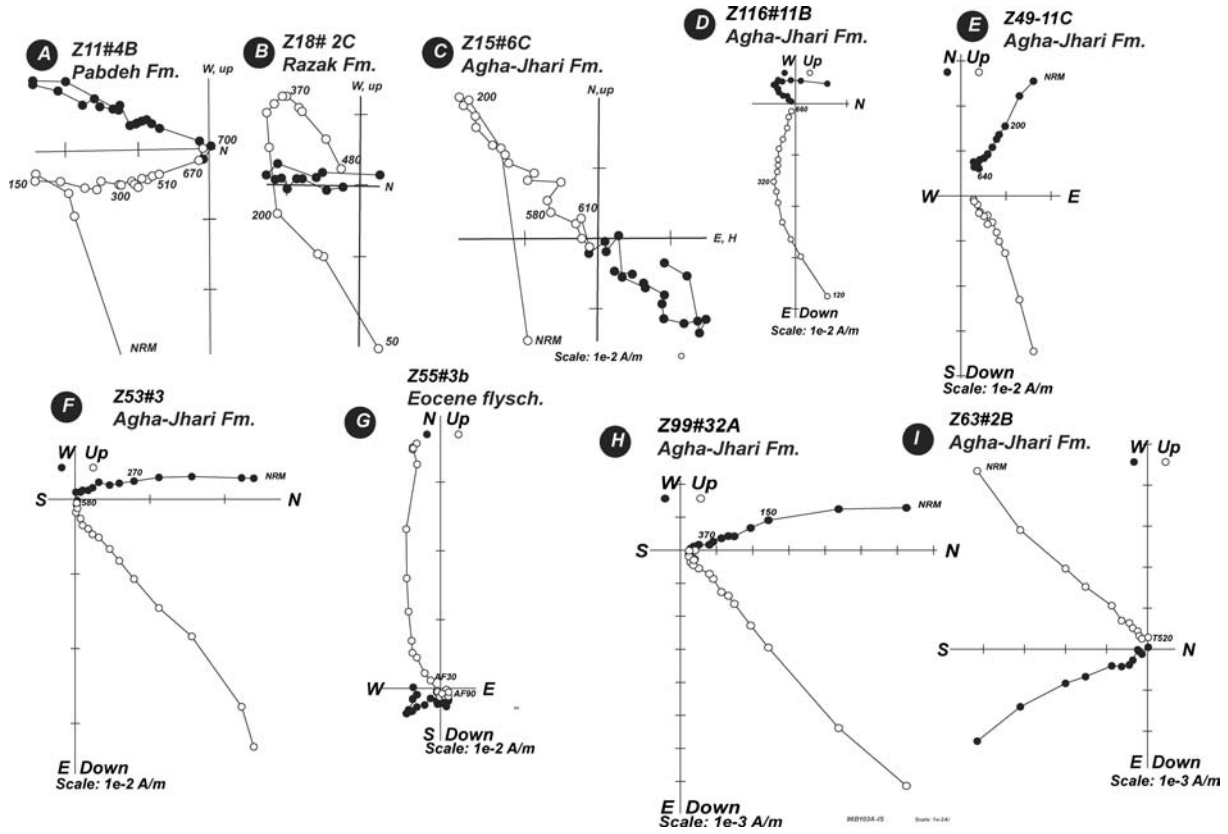

Figure 4. Representative orthogonal plots during thermal demagnetization. Black (open) symbols are the horizontal (vertical) projection. *In situ* coordinates. All these samples have been thermally demagnetized (temperature is indicated) except sample Z54#3B where AF demagnetizations is shown (values in mT).

In the Oligocene Razak Fm., ten sites have been investigated (Fig. 5c, Table 1). Four sites provide component A (Table 1). The unblocking temperatures are either characteristic of viscous magnetization (Z5, Z20) or can have the highest unblocking temperatures (Z6) or unblocking fields (Z28). Six sites show a component B. The polarity is essentially normal except at site Z23, with exclusively reverse polarity, and sites Z9 and Z18 where mixed polarities are observed (Fig. 4b). The B component spans any unblocking temperatures range (Z18), or unblocking fields up to 100 mT (Z24). As can be seen in Fig. 5c and Table 1, the component B direction is ill-defined in site Z9 ($\alpha_{95} = 23^\circ$) and questionable in sites Z24 and Z16, because, respectively, close to vertical and to horizontal, in any coordinate system. The magnetization of the sites with reversed polarity (Z18 and Z23) can be ante, syn or post-tectonic as well. It is probably syntectonic at site Z17.

In the Oligo-Miocene Guri Fm., sites Z31 and Z33 (Table 1) provide component A and component B, respectively. Component B has two polarities in the high-temperature range, but the magnetization is very weak in this Formation, making difficult to determine a characteristic direction. At site Z33, component B would rather be post-tilting (Fig. 5c, Table 1). Site 19 in the lower Miocene Mishan Fm. has only an A component (Table 1), insignificantly deviated to the west.

Ten sites are investigated in the Mio-Pliocene Agha-Jhari formation (Fig. 5d). Five sites have only a component A, sometimes with high unblocking temperatures, as in sites Z14 and Z22. As inclination after bedding correction is consistent with the expected inclinations, component A at sites Z14 and Z22 can be a syn- to pre tilting magnetization. Except at sites Z15 and Z32 where a reverse polarity is observed (Fig. 4c), the component B is characterized by normal polarity at sites Z21, Z27 and Z29. The maximum unblocking temperatures are 600 °C. After complete bedding correction, the mean inclination and its standard deviation is $37 \pm 21^\circ$. Although ill-defined, the mean inclination is comparable to mean inclination obtained in Agha-Jhari Fm. (Homke *et al.* 2004; Smith *et al.* 2005) This observation, together with the occurrence of normal and reverse polarities pleads for a pre-tilting origin of component B. Note that no large deviation of component B with respect to geographic north is observed, except at site Z21.

Eastern Fars Arc and western part of ZMS

We present results in twenty four sites all sampled in the Mio-Pliocene Agha-Jhari Fm. Six sites exhibit component A (Fig. 5a). Among them, two have high unblocking temperatures up to 700 °C (sites Z37 and Z83), but their inclination is more consistent with the present-day inclination in geographic coordinates than after bedding correction. Eighteen sites display component B with mixed polarities (Figs 4d and e, 5e). After bedding correction, inclination is ranging from 61° to 2°, with a mean value at $28^\circ \pm 18^\circ$, that is, lower to what observed in western Fars Arc for Agha-Jhari rocks. This would suggest that component B is possibly syn-tilting, or affected by inclination error. Ten and four sites display, respectively, a counter-clockwise and clockwise deviations of component B both in geographic coordinates and after bedding correction. After bedding correction, two sites show no significant deviation of component B, and two sites show strong deviation of component B.

Table 1. Palaeomagnetic components. C: type of component. λ: latitude; θ: longitude; *n*: number of samples used for the mean direction analysis. Range of temperature or AF magnetic field is indicated. *D*: Declination. *I*: inclination. *K* and α_{95} are, respectively, the precision parameter and half confidence angle from Fisher (Fischer 1953) statistics. Components are indicated *in situ* (geographic coordinate) and after full bedding correction.

West Fars Arc														
							In situ				*After bedding correction*			
Site	C	λ	θ	*n*	Age	Range	*D*	*I*	*K*	α_{95}	*D*	*I*	*K*	α_{95}
Z-10	*B*	28°54′	52°19′	7	Pabdeh	100–400 °C	176	−21	8	25	179	−56	17	17
Z-11	*B*	28°54′	52°29′	6	Pabdeh	100–700 °C	214	4	42	10	215	−25	42	10
Z-2	*A*	28°53′	52°19′	6	Asmari Fm.	NRM-100 mT	358	42	104	8	3	60	98	8
Z-3	*B*	28°55′	52°30′	3	Asmari Fm.	NRM-500 °C	330	32	24	26	329	26	25	25
Z-4	*A*	28°55′	52°30′	6	Asmari Fm.	NRM-300 °C	9	45	81	7	11	20	74	7
Z-5	*A*	29°05′	52°35′	6	Razak Fm.	NRM-300°C	0	46	549	3	262	48	548	3
Z-6	*A*	29°37′	52°39′	7	Razak Fm.	NRM-650 °C	8	55	70	8	8	−4	72	8
Z-9	*B*	28°53′	52°36′	9	Razak Fm.	100–300 °C	55	56	10	23	67	58	10	23
Z-16	*B*	28°49′	52°44′	8	Razak Fm.	NRM-400 °C	18	11	12	17	19	14	12	17
Z-17	*B*	28°41′	52°58′	5	Razak Fm.	120–400 °C	327	72	20	16	2	27	20	16
Z-18	*B*	28°27′	53°07′	4	Razak Fm.	400–700 °C	187	−39	2942	2	191	−54	2987	2
Z-20	*A*	28°30′	53°33′	10	Razak Fm.	NRM-300 °C	4	40	29	10	4	48	29	10
Z-23	*B*	28°41′	53°51′	8	Razak Fm.	NRM-500 °C	161	−43	97	6	173	−38	95	6
Z-24	*B*	28°49′	54°01′	6	Razak Fm.	NRM-100 mT	32	68	55	12	18	78	59	11
Z-28	*A*	28°21′	54°03′	5	Razak Fm.	NRM-100 mT	15	54	105	8	186	81	113	7
Z-31	*A*	27°43′	54°07′	5	Guri Fm.	NRM-100 mT	6	38	97	7	8	35	97	7
Z-33	*B*	27°24′	54°07′	6	Guri Fm.	120–600 °C	172	−48	45	11	195	−58	54	10
Z-19	*A*	28°27′	53°23′	8	Mishan Fm.	120–500 °C	349	45	19	15	3	12	19	15
Z-14	*A*	28°54′	51°58′	8	Agha-Jhari Fm.	100–500 °C	359	40	178	4	342	53	178	4
Z-15	*B*	28°56′	51°59′	6	Agha-Jhari Fm.	NRM-500 °C	143	−47	21	14	156	−45	21	14
Z-21	*B*	28°32′	53°35′	6	Agha-Jhari Fm.	120–450 °C	90	1	62	9	110	41	62	9
Z-22	*A*	28°40′	53°44′	7	Agha-Jhari Fm.	120–700 °C	350	37	25	13	9	39	26	13
Z-26	*A*	28°31′	54°14′	4	Agha-Jhari Fm.	NRM-250 °C	354	48	104	8	354	12	68	10
Z-27	*B*	28°26′	54°10′	10	Agha-Jhari Fm.	100–500 °C	29	33	6	24	27	4	6	24
Z-29	*B*	28°02′	54°00′	6	Agha-Jhari Fm.	120–450 °C	31	67	26	17	22	33	26	17
Z-30	*A*	27°46′	54°01′	9	Agha-Jhari Fm.	NRM-200 °C	4	38	42	8	5	−1	43	8
Z-32	*B*	27°35′	54°09′	5	Agha-Jhari Fm.	NRM-400 °C	180	−16	26	15	177	−62	26	15
Z-34	*A*	27°09′	54°09′	10	Agha-Jhari Fm.	100–500 °C	356	47	68	6	355	22	67	6
West ZMS														
							D	*I*	*K*	α_{95}	*D*	*I*	*K*	α_{95}
*Z*36	*A*	27°30′	56°11′	7	Agha Jhari Fm.	NRM-100 mT	349	52	20	17	13	86	21	16
*Z*37	*A*	27°37′	56°11′	9	Agha Jhari Fm.	NRM–700 °C	355	50	99	5	351	11	57	7
*Z*38	*A*	27°45′	56°05′	9	Agha Jhari Fm.	120–350 °C	4	45	135	5	4	23	133	5
*Z*39	*B*	27°53′	55°59′	5	Agha Jhari Fm.	120–600°C	340	1	85	9	341	19	85	9
*Z*40	*B*	28°14′	55°50′	6	Agha Jhari Fm.	120–300 °C	191	−41	16	15	200	−20	16	15
*Z*41	*A*	28°16′	55°51′	10	Agha Jhari Fm.	NRM–300 °C	0	47	206	4	221	22	35	9
*Z*42	*A*	28°18′	55°53′	7	Agha Jhari Fm.	NRM-350°C	351	46	61	10	231	44	60	10
*Z*44	*B*	27°29′	56°21′	5	Agha Jhari Fm.	200–700 °C	341	27	43	19	331	41	43	19
*Z*46	*B*	27°33′	56°28′	6	Agha Jhari Fm.	350–680 °C	0	23	43	10	63	−61	44	10
*Z*47	*B*	27°31′	56°28′	3	Agha Jhari Fm.	520–695 °C	151	28	545	5	152	−21	545	5
*Z*48	*B*	27°29′	56°23′	4	Agha Jhari Fm.	360–695 °C	23	−16	127	8	23	25	127	8
*Z*49	*B*	27°27′	56°26′	6	Agha Jhari Fm.	200–680 °C	30	46	59	9	33	50	59	8
*Z*73	*B*	27°17′	56°13′	9	Agha Jhari Fm.	300–695 °C	337	26	27	10	336	16	27	10
*Z*80	*B*	27°18′	56°04′	4	Agha Jhari Fm.	100–400 °C	346	36	194	3	16	36	194	3
*Z*81	*B*	27°20′	56°09′	4	Agha Jhari Fm.	300–630 °C	340	36	43	14	347	53	43	14
*Z*82	*B*	27°17′	56°18′	5	Agha Jhari Fm.	400–660 °C	333	27	18	19	331	21	18	19
*Z*83	*A*	26°51′	55°23′	6	Agha Jhari Fm.	NRM–695 °C	355	48	12	21	353	28	12	21
*Z*84	*B*	26°43′	55°09′	3	Agha Jhari Fm.	NRM–695 °C	193	12	593	5	194	−18	593	5
*Z*86	*B*	27°46′	56°00′	5	Agha Jhari Fm.	500–695 °C	180	55	14	21	180	−13	14	21
*Z*87	*B*	N27°32′56″	E56°27′06″	8	Agha Jhari Fm.	500–695 °C	140	15	45	14	137	−12	49	13
*Z*89	*B*	N27°35′59″	E56°17′31″	4	Agha Jhari Fm.	230–600 °C	328	41	63	16	327	2	102	12
*Z*91	*B*	N27°42′07″	E56°26′05″	3	Agha Jhari Fm.	380–680 °C	39	24	28	24	80	58	37	21
*Z*116	*B*	N27°32′23″	E56°44′07″	5	Agha Jhari Fm.	520–660 °C	199	67	55	10	178	−23	69	9
*Z*117	*B*	N27°08′57″	E56°03′17″	5	Agha Jhari Fm.	440–600 °C	95	44	30	14	102	2	30	14

Table 1. (*Continued.*)

						East ZMS								
Northern part of east syntaxis							*D*	*I*	*K*	α95	*D*	*I*	*K*	α95
*Z*53	*B*	56°58′	27°26′	5	Agha Jhari Fm.	100–605 °C	325	46	69	9	359	6	59	19
*Z*54	*B*	56°57′	27°22′	7	Agha Jhari Fm.	150–605 °C	332	53	71	7	284	46	74	7
*Z*55	*B*	57°18′	26°51′	3	Eocene flysch	100–600 °C A	273	−81	272	8	242	−54	74	14
Southern part of east syntaxis														
*Z*99	*B*	N26°05′57″	E57°16′12″	14	Agha Jhari Fm.	150–500 °C	347	51	127	4	16	34	127	4
*Z*100	*A*	N26°06′35″	E57°17′05″	12	Agha Jhari Fm.	200–500 °C	1	41	60	6	349	46	68	5
*Z*71	*B*	57°14′	26°12′	5	Agha Jhari Fm.	100–460 °C	347	48	22	17	316	36	22	17
*Z*66	*B*	57°36′	25°50′	6	Agha Jhari Fm.	NRM–400 °C	42	33	29	13	48	39	29	13
*Z*63	*B*	57°55′	25°56′	6	Agha Jhari Fm.	5–35 mT, 120–5	351	44	97	7	327	57	48	10
*Z*62	*B*	57°55′	26°05′	4	Agha Jhari Fm.	NRM-10 mT, 36	334	39	66	11	341	58	65	11
*Z*61	*B*	57°49′	25°49′	3	Agha Jhari Fm.	NRM-100 mT	132	−24	35	21	133	−20	35	21

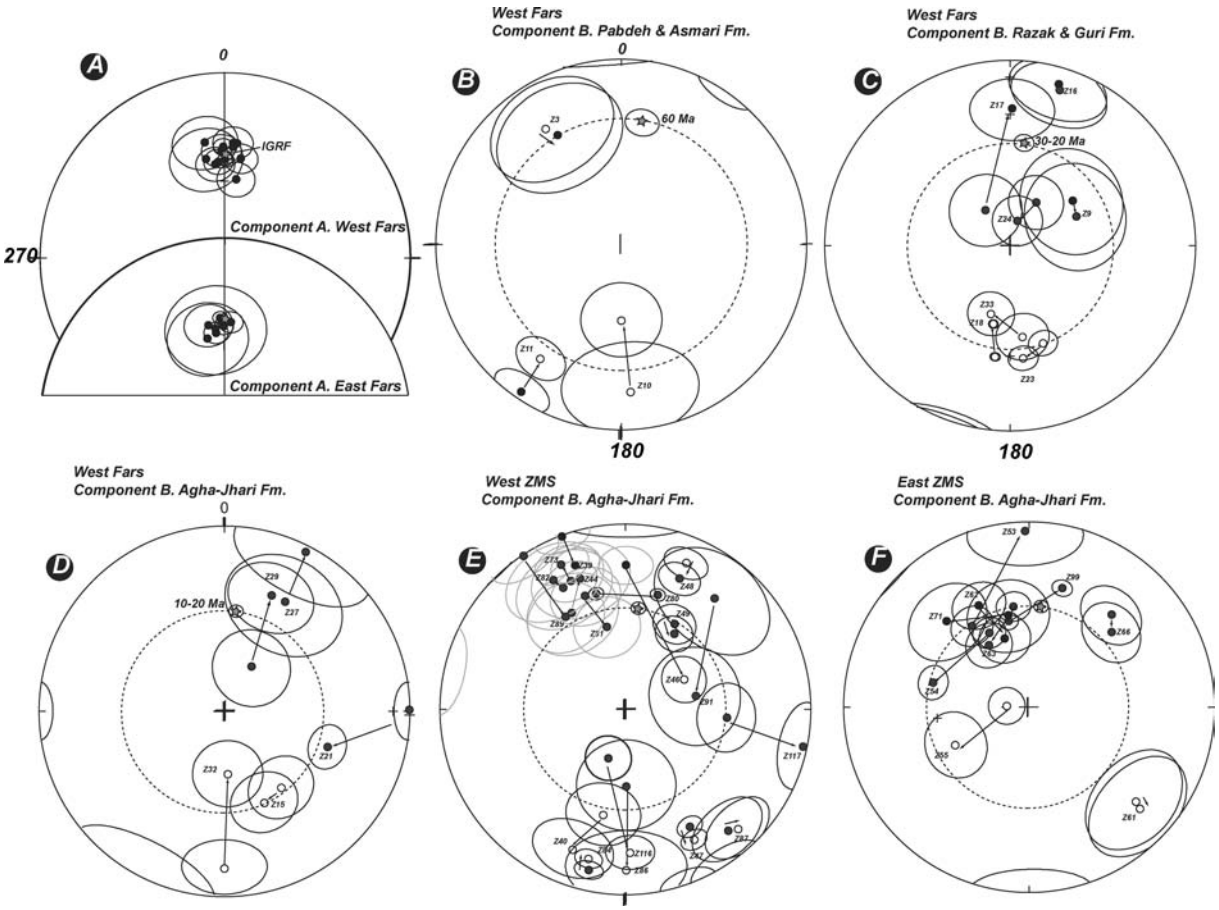

Figure 5. Equal area projection of the mean component directions before and after bedding correction with their confidence angle at 95 per cent. An arrow shows the path from geographic to tectonic coordinates. Black (open) symbols are plotted in the lower (upper) equal area projection. The direction of IGRF is indicated for components A (star).We also plot the reference direction (grey stars) expected from the APWP for Africa proposed by Besse & Courtillot (1991). Dashed circles show the expected inclination.

Eastern part of ZMS

We sampled all sites in the Mio-Pliocene rocks of the Agha-Jhari Formation. In the northern part of this area, roughly north from N27° latitude, these rocks are reddish sandstones to marly siltstones, like in the western part of the syntaxis. However, south from N27° the Agha-Jhari Fm. becomes more marly, and reddish sandstones disappear. We first examine the northern part, then the southern part of the eastern syntaxis.

In the northern part of ZMS, Smith *et al.* (2005) studied seven sites across the sigmoidal Minab fold. There, a pre-tilting ChRM carried by magnetite and hematite has been recorded in fine-grained silstones of the Agha-Jhari formation. In the present study, we report two additional sites within the Minab fold (sites Z53 and Z54, Figs 4f and 5f). They consist in coarse grained red sandstone and are characterized by a B component of normal polarity in the range 100–600 °C. This component B at sites Z53 and site Z54 is better grouped in geographic coordinates (Fig. 5f). Site Z55 is sampled

in Eocene flysch along the Zendan fault. A steep component B (Fig. 4g) is observed in geographic coordinates (Table 1).

In the southern part of eastern ZMS, we report results of 7 sites, all sampled in Agha-Jhari Fm. (Fig. 5f). Site Z71 displays an ill-defined component B. Sites Z99 and Z100 belongs to the same fold. Components A and B are detected, respectively, at sites Z100 and Z99 (Fig. 4h). At site Z66, a component B is easterly deviated (Table 1). Sites Z61, Z62 and Z63 (Fig. 4i) have a component B defined by a limited number of samples. Mixed polarities and a west declination characterize Component B . All components B, except those of sites Z55, Z66 and Z99 are westerly deviated. It is noticeable that components B at sites Z62, Z63, Z71, Z99, Z53 and Z54 are close to each other in geographic coordinates, and split apart after bedding correction.

DISCUSSION

We report 42 components B to propose a first pattern of block rotations in the Fars arc and the ZMS. The relatively large occurrence of component A shows that post folding remagnetization is frequent in Zagros, particularly in coarse grains clastics rocks. This remagnetization can hide reversals sequences and thus limits the application of magnetostratigraphy in the Fars Arc.

The origin of component B

Component B can be a primary component or a remagnetization. The use of fold test can help to date component B. Unfortunately, in the present study, only few sites are suitable for a fold test because of our initial sampling scheme. This is particularly true in the western Fars Arc where complementary work is in progress to provide well-constrained fold tests.

In the western Fars Arc, component B is likely pre-tilting when considering the inclination after bedding correction. Indeed, inclination in Pabdeh and Asmari formations is better consistent with Palaeocene-Oligocene inclination after bedding correction (Fig. 5b). In Razak and Guri formations (Fig. 5c), the directions with reverse and normal polarities of components B are, respectively, well defined and poorly defined. Although the dip of bedding of reverse components B is small, the inclination of normal and reverse polarities are consistent with expected inclination after bedding correction. We therefore, interpret components B in Razak Fm. and Guri Fm. as pre-tilting. In Agha-Jhari formation, the inclinations are also more consistent after bedding correction (Fig. 5d) for four sites.

In ZMS, the component B from Agha-Jhari formation can be either pre-tilting or post-tilting. In the western ZMS, the Namak and Siah folds, both located north of Bandar Abbas, have been sampled in different places, allowing the application of a fold test (localisation of these fold is shown Fig. 6). The pattern of palaeomagnetic deviation is contrasting. Four sites show counter-clockwise deviation (sites Z89, Z87, Z46 and Z47) and two sites show clockwise deviation (sites Z48, Z49) (Fig. 6). The latter two are situated in the southern flank of Siah fold. The $\sim 120^{\circ}$ strong deviation observed at site Z46 is questionable as no evident geological observation can explain such contrasting amplitude with respect to neighbour sites. Note that a south dipping E–W thrust separates the Siah and Namak folds (Molinaro *et al.* 2005) (Fig. 6). This thrust can be the result of opposite block rotations of the two folds Namak and Siah. We apply the fold test for sites showing the same declination deviation (Z89–Z87–Z47 and Z48–Z49). The result of fold test suggests a pre-tilting acquisition of component B (Figs 7a and b). At the southern limb of Siah fold (Fig. 7b), the inclination of component B after bedding correction is consistent with other published results (Homke *et al.* 2004; Smith *et al.* 2005). At Namak fold and from the northern

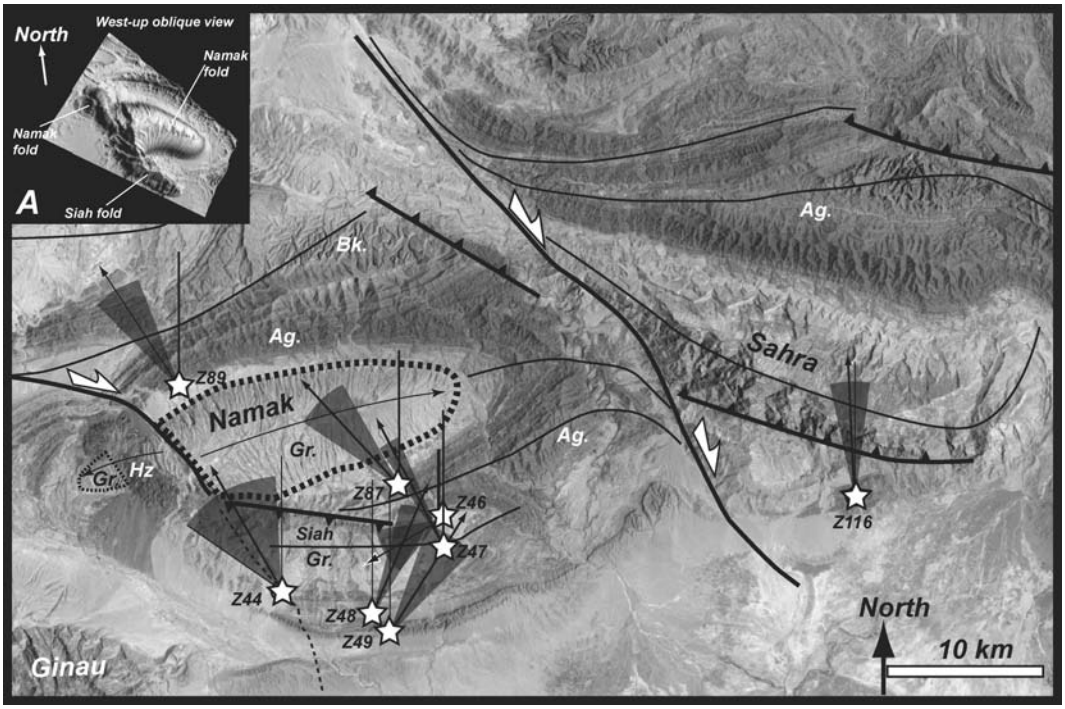

Figure 6. Close up of component B after bedding correction in the Namak fold. The direction is shown with respect to its reference declination. The fan of error corresponds to the wide of confidence circle when plotted in lower hemisphere. Image Landsat 6. We show the trace of faults (thick lines) and folds axes (thin lines). Bk: Bakhtiari Fm., Ag.: Agha-Jhari Fm., Gr.: Guri Fm., Hz: Hormuz salt. Inset: Namak fold viewed from the west, up. The right lateral offset of western termination of Namak fold is thus apparent.

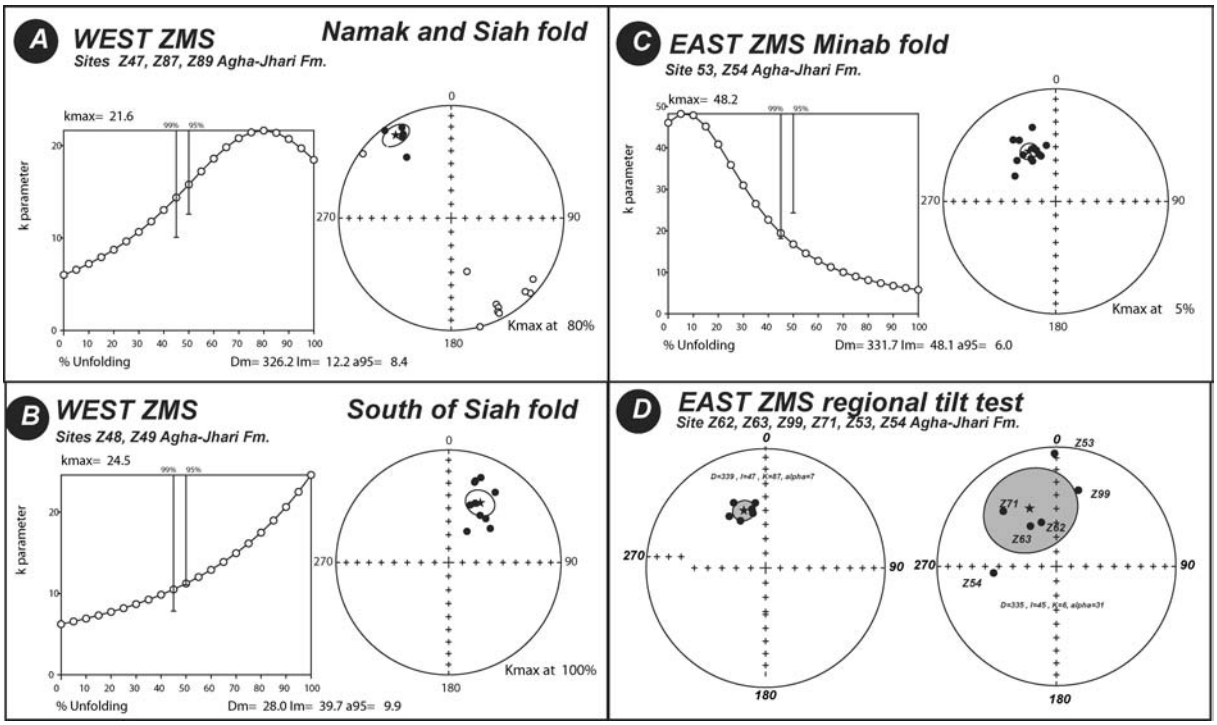

Figure 7. Fold tests using Palaeomac software (Cogné 2003) in the syntaxis. Equal area projection. Same conventions as in Fig. 5. (a) Namak fold. (b). Siah fold. (c) Minab fold north of east ZMS. (d) Regional tilt test in the southern part of east syntaxis. Site mean directions in D.

limb of Siah fold, however, the inclination is too low by about ∼25° (Fig. 7a). There are several possible explanations for this abnormal inclination. The component B in this fold can be poorly recovered, and its determination is questionable. More likely, the low inclination can be attributed to hematite as it is frequently observed in hematite bearing rocks from the Middle East (Chauvin *et al.* 1996).

In the eastern ZMS, Smith *et al.* (2005) showed that component B in Agha-Jahri formation is pre-tilting. The Eocene flysch site Z55, which is located near the Zendan fault, shows an easterly deviated component B that is likely pre-tilting according to the inclination (Fig. 5f). However, in both limbs of the Minab fold (sites Z53 and Z54), our B component is a post-tilting remagnetization as attested by the fold test (Fig. 7c). We applied a regional tilt test to the components B at sites Z62, Z63, Z99, Z71, Z53 and Z54 from the east ZMS and Makran Arc. All components B are grouped in the NW quadrant before bedding correction (Fig. 7d). The site mean components B scatter upon dip correction, demonstrating, therefore, their post-tilting origin. The mean *in situ* direction ($D = 339°$; $I = 47°$; $K = 87$; $\alpha_{95} = 7°$) is comparable to the remagnetization component A' reported by Smith *et al.* (2005) from site Z51 of the Minab fold.

Rotation along vertical axis

We plot declinations of components B through the western Fars Arc (Fig. 8) and the ZMS (Fig. 9). We plot components B after bedding correction through the Fars Arc, except at some sites in the eastern part of the ZMS where we identified post-tilting component B. For Asmari and Pabdeh formations, we used a declination reference of N10°, according to the reference of directions calculated from the APWP. For rocks belonging to the Fars group, younger than Oligocene, we used the present-day direction of the north because the expected direction are not significantly different from the present dipole.

In the western part of Fars Arc (Fig. 8a), two components B (Z10, Z17) show slight counter-clockwise deviation (<10°). Six components B are much more statistically deviated; two and four are deviated, respectively, counter-clockwise (Z15 and Z3) and clockwise (Z9, Z11, Z16 and Z18). In the Central Fars Arc (Fig. 8b), five sites (Z21, Z24, Z27, Z29 and Z33) display clockwise deviations of component B, one counter-clockwise deviation (Z23), and one not significantly deviated (Z32).

West of ZMS (Fig. 9), two sites display component B with no significant deviation (Z86 and Z116). Six sites have their component B clockwise deviated (Z40, Z48, Z49, Z80, Z84 and Z91). A much larger number of sites have their component B counter-clockwise deviated (Z39, Z44, Z46, Z47, Z73, Z81, Z82, Z87, Z89 and Z117).

East of ZMS (Fig. 9), we distinguish pre-tilting and *in situ* component B. For pre-tilting component B, including Smith *et al.* (2005) data, we observe seven clockwise deviations (Z110, Z111, Z112, Z113, Z114, Z55 and Z66) and one counter-clockwise deviation (Z61). For *in situ* component B, six sites show a ∼20° post-folding counter-clockwise deviation.

Structural significance of block rotation

As a whole, no large deviations (>∼40°) are observed except at sites Z21, Z117 and Z46. Hence, one can state that no large rotation affect the Fars arc since the Palaeocene to Mio-Pliocene.

In the western part of Fars arc, clockwise rotations dominate apparently the pattern (nine clockwise against three counter-clockwise). Local rotations due to strike slip fault motion are likely as folds show often torsion in the vicinity of these faults (Authemayou *et al.* 2006). This is particularly true near the Mangarak fault (Fig. 10). There, the deviation of component B follows more or less the trend of the bended fold. This supports the concept of local rotations induced by the torsion of the fold due to strike

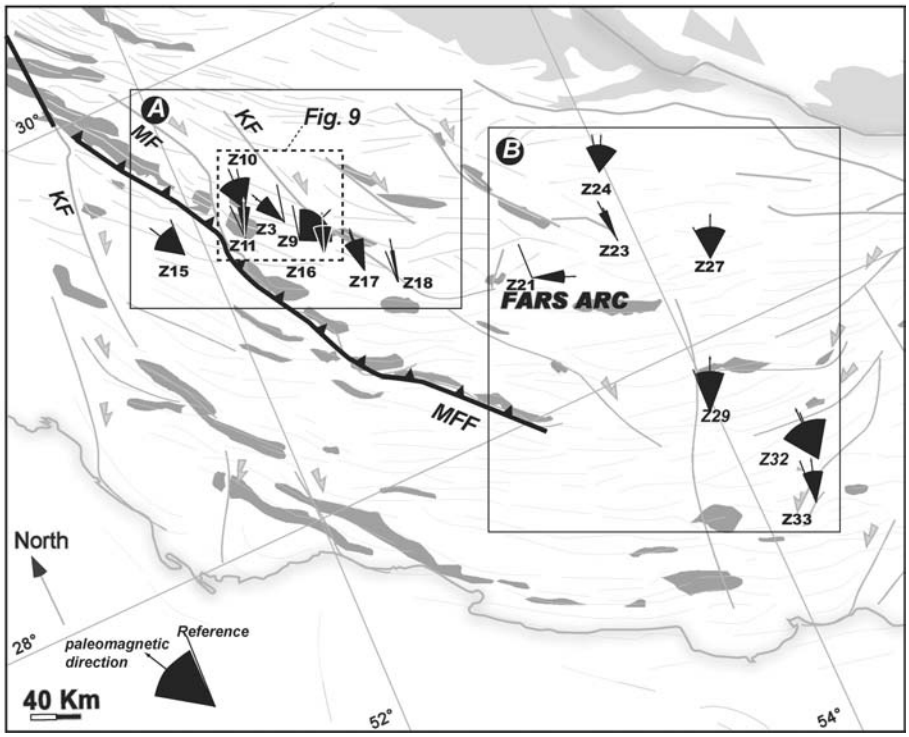

Figure 8. Map of component B declinations after bedding correction in the western Fars Arc. Same convention as in Fig. 6. A and B areas are discussed in the text. Reference direction is ∼N10 for Pabdeh to Asmari Fm. and ∼N0 for younger formations. KF: Kazerun fault, MF: Mangarak fault; KF: Karebas fault; MFF: Mountain front fault.

slip motion as sketched in Figs 3b–e. This observation in this fold is different from the results obtained in the Minab fold (Eastern part of the ZMS), where it is demonstrated that the torsion of the fold is not accompanied by differential rotations of its different parts (see Figs 3d–g) (Smith *et al.* 2005). Given the large occurrence of strike slip displacement in western Fars Arc (Berberian 1995; Authemayou *et al.* 2006), we expect that local rotations induced by faults is a frequent phenomenon. The observation of counter-clockwise rotations suggest that either left lateral faults may have played a role; or that it is a result of dextral strike slip fault as discussed by Authemayou *et al.* (2006). Note that left lateral faults are not yet clearly identified in the western Fars Arc.

From this study, we cannot decipher about possible regional scale rotation in the western Fars Arc as predicted by several studies (Bakhtari *et al.* 1998; Hessami *et al.* 2001a; Talebian & Jackson 2004; Authemayou *et al.* 2006; Lacombe *et al.* 2006). Current palaeomagnetic work is in progress to precise the pattern of block rotations in the western Fars Arc.

In the ZMS, the counter-clockwise and clockwise rotations dominate in the western and eastern sides, respectively. Note that site Z116, which is in the central part of the syntaxis shows no deviation of component B. The dominant sense of block rotation in the western ZMS agrees with the predictions of Molinaro *et al.* (2005) and Sepher & Cosgrove (2004) and thus disagrees with Hessami *et al.* (2001b).

At first glance, the principal pattern of block rotation suggests that the pronounced shape of ZMS is acquired, or amplified, secondary. This pattern is consistent with the model of the two arcs development (Zagros and Makran) proposed by Molinaro *et al.* (2005). This pattern is also consistent with rotations expected in the shear band systems along each side of the ZMS (Furst 1990; Cosgrove & Ameen 2000; Aubourg *et al.* 2004). At Namak fold, palaeomagnetic and structural data are consistent with a domino-like pattern block rotation (Ron *et al.* 1984), and thus is compatible with the shear band hypothesis. From field and photo inspections, we propose that right lateral strike slip faults bound the Namak fold (Aubourg *et al.* 2004) (Fig. 6). In a domino-like pattern, the right-lateral strike slip faults can be interpreted as the result of relative displacement of individual blocks during counter-clockwise rotation; this counter-clockwise rotation being the response of a regional left lateral wrench shear.

The pattern of pre-tilting component B (sites Z66 and Z61) in the southern part of east ZMS (Fig. 9) suggests that the western termination of the Makran Arc is acquired or amplified secondary. However, we miss data to better illustrate this torsion. One intriguing result obtained in this study is certainly the pattern of post-folding component B along the East ZMS (Fig. 9). The post-folding ∼20° counter-clockwise rotation does not contradict the clockwise rotation illustrated by pre-tilting components B, particularly in the Minab fold, but suggests that initial clockwise rotation is of higher magnitude. Thus, the clockwise rotation of the Minab fold would be of about ∼40° rather than ∼20° as observed from pre-tilting component B. We have no explanation to account for this temporal succession of clockwise and counter-clockwise rotations along the eastern ZMS.

We now propose to compare palaeomagnetic rotations to present-day rotations. Bayer *et al.* (2006) presented the tensor of rotation deduced from GPS network in the ZMS and east Makran. They report rotation rates ranging from ∼1 to ∼6 deg Myr^{-1} in the ZMS and eastern Makran. Given this range of rate, no block rotation larger than 30° is expected since the Miocene. This is consistent with palaeomagnetic data obtained in Agha-Jhari Fm. Active rotations are predominantly counter-clockwise and clockwise, west and east of ZMS, respectively, (Fig. 9). There is some agreement between the whole pattern of palaeomagnetic data and

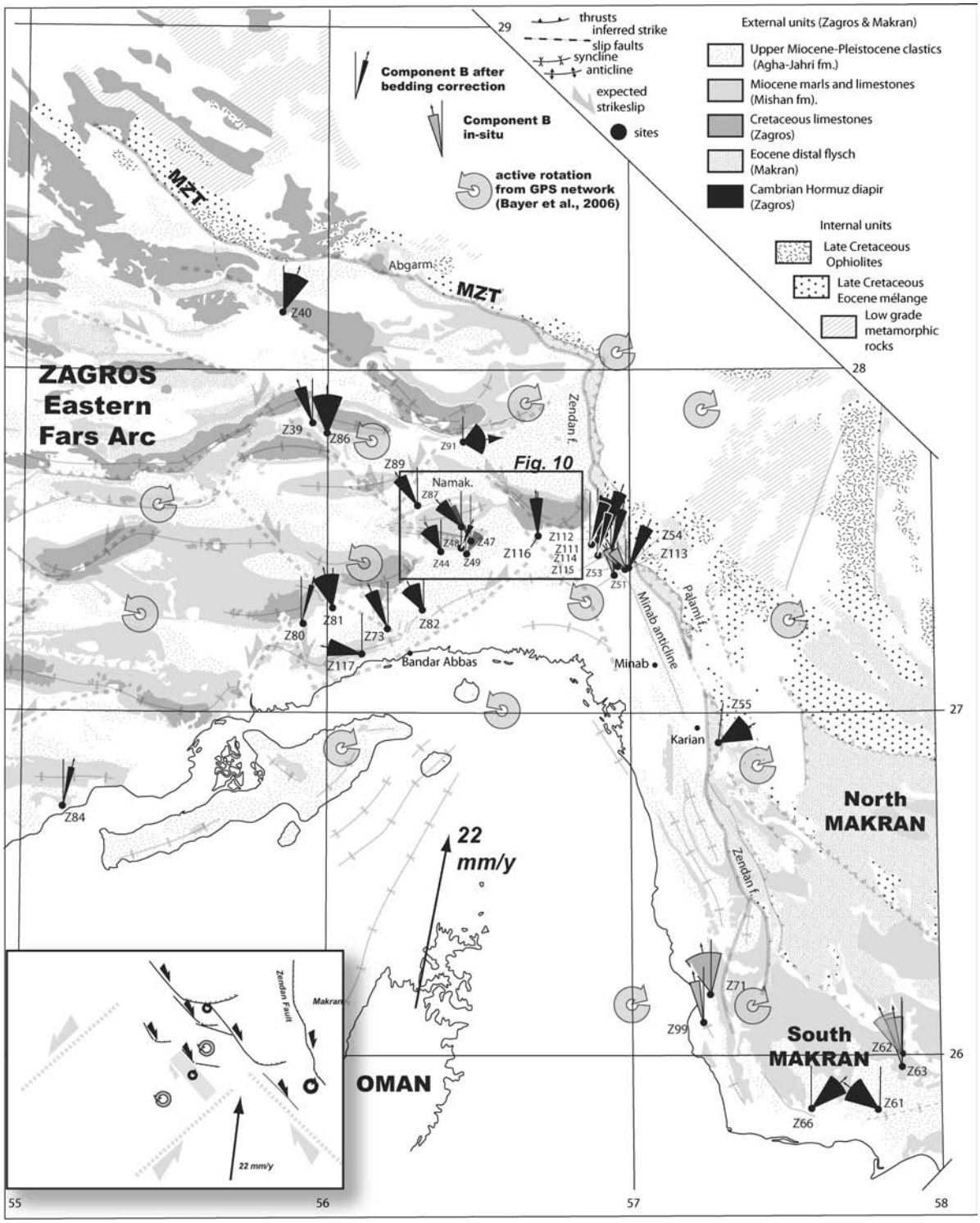

Figure 9. Map of component B declinations in the syntaxis. B components are plotted before or after bedding correction. We add Smith *et al.* (2005) pre-tilting component in the Minab fold. Inset: cartoon illustrating the major tectonic faults and block rotations in the syntaxis.

GPS rotation tensors in ZMS. Interestingly, Bayer *et al.* (2006) report counter-clockwise rotation in the area of Minab, eastern ZMS (Fig. 9). This counter-clockwise rotation matches to the western deviation of post-folding component B (Fig. 9) although we miss more data to elucidate this pattern.

We propose a scenario of tectonic evolution of the ZMS from Mio-Pliocene to present time (Fig. 11). During Mio-Pliocene (Fig. 11a), the Agha-Jhari formation was deposited along ∼W–E direction in the area of future ZMS. At that time, the Zendan fault acted probably as a thrust, striking ∼SE–NW, and separating Zagros (continental collision) from Makran accretionary prism (oceanic subduction). This interpretation is consistent with the palaeostress data proposed by Regard *et al.* (2004) and the balanced cross-sections in the Minab fold built by Molinaro *et al.* (2004). In those balanced cross-sections,

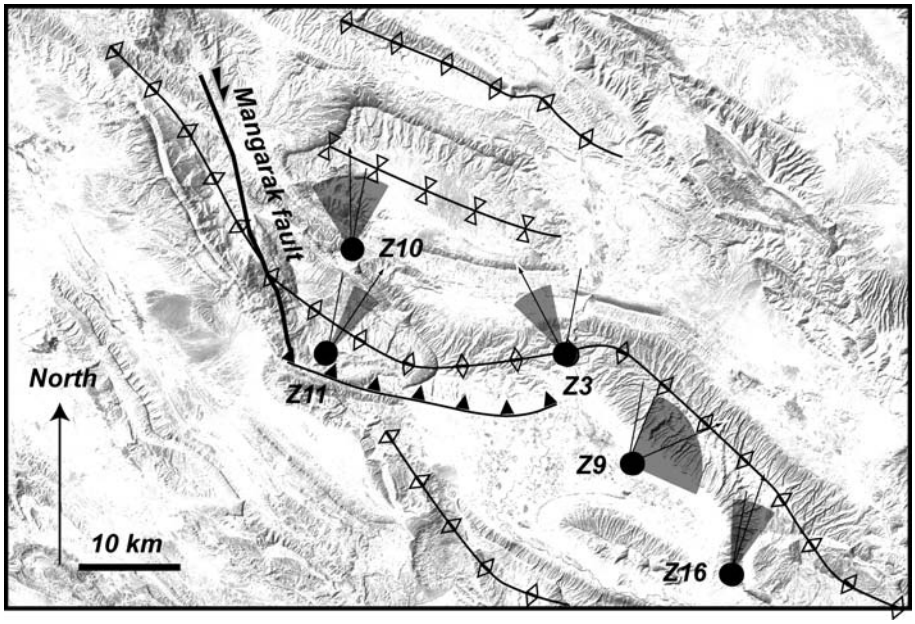

Figure 10. Close up of B component after bedding correction in a disrupted fold in the vicinity of the Mangarak dextral strike slip fault and the Mountain Front Fault. The shaded topography results from Landsat 6 image. Location of this structure is also indicated in Fig. 3b and Fig. 8.

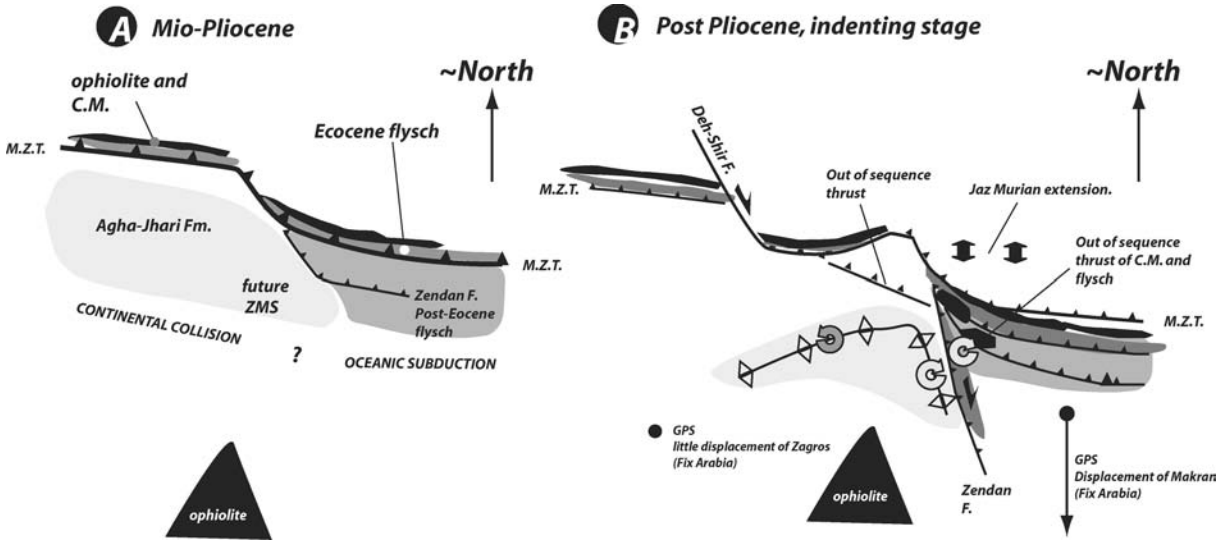

Figure 11. Cartoons showing the Mio-Pliocene (a) to post Pliocene evolution (b) of the Zagros Makran syntaxis. The E-W trending of Agha-jhari is schematic and concerns only the eastern termination of Zagros belt. See explanations in the text. C.M. coloured mélange.

the Zendan fault is a flat east-dipping thrust, implying that the limit between Zagros and Makran is located eastward of Zendan Fault. We adopt in our model a 'dog-leg' shape of the Main Zagros Thrust and the Zendan fault in order to limit the amplitude of rotation along vertical axis. This initial bended shape is also consistent with experimental modelling of the collision between continental lithospheres that took place in the Zagros, and the subduction of oceanic lithosphere beneath up-lifted Makran accretional prism (Regard *et al.* 2005).

After the Pliocene (Fig. 11b), we propose an indenting stage of the syntaxis area. We emphasize particularly the assumed role of Oman belt that plays as an obstacle to the free propagation of the Zagros belt. Therefore, Oman belt can be seen as an indenter. Such interpretation has been supported by several authors (Kadinski-Cade & Barazangi 1982; Aubourg *et al.* 2004; Sepehr & Cosgrove 2004; Smith *et al.* 2005; Bayer *et al.* 2006). Bayer *et al.* (2006) suggest also that Oman promontory is subducting beneath ZMS. Indeed, GPS data in the frame of fix Arabia shows that Zagros is relatively fixed while Makran is moving southward (Fig. 11b) (Vernant *et al.* 2004; Bayer *et al.* 2006). The transpressive Zendan fault is one of the major fault which participate to the decoupling between Zagros and mobile Makran belt (Regard *et al.* 2004). Our model suggests an apparent $\sim 45^\circ$ clockwise rotation of the Zendan fault, which is not supported by palaeomagnetic data from the Zagros stripe along the Zendan fault where $\sim 20^\circ$ is recorded by Agha-Jhari Fm.. This apparent contradiction can be solved out in assuming a gradient of thrust displacement along the Zendan fault positive from north to south during indentation. Rather than indentation imposed by Oman

indenter, Molinaro *et al.* (2004) proposed that ZMS results from the convergence of Zagros and Makran belts. However, we think that indentation is a dominant process as the present-day coast of the syntaxis and the envelope of folds mimic the Oman peninsula shape (e.g. Fig. 1a) (Aubourg *et al.* 2004).

We attempt to relate several geological structures during this indenting stage (Fig. 11b). First, palaeomagnetic data suggest that the present-day V-shape of ZMS is thus acquired or amplified secondary, after the deposition of Agha-Jhari Fm.. Secondly, the southern propagation of the Makran prism relative to the Zagros belt can explain the clockwise bending of flysch belt towards the Zendan fault and transpression along the Zendan fault. We thus suggest that the eastern Makran arc is acquired, or amplified, secondary during the relative propagation of the Makran along the Zendan fault. In addition, we propose to relate the propagation of the Makran prism and the Plio-Pleistocene opening of the Jaz Murian basin (Fig. 11b). Thirdly, the convergence of major faults (High Zagros fault, Main Front fault, Zagros Front fault) in the core of the syntaxis (Fig. 2) has been amplified probably during the indenting stage. In this logic, the out of sequence basement fault north of the syntaxis (Fig. 11b) proposed by Molinaro *et al.* (2005) would be related to the indenting stage of the syntaxis.

CONCLUSION

The present palaeomagnetic study deals with rocks from Palaeocene to Mio-Pliocene age, sampled extensively throughout the Fars Arc and in the Zagros-Makran syntaxis. The large majority of the collection concerns coarse-grained sandstone and siltstone of the Agha-Jhari Mio-Pliocene Formation. Recent remagnetizations close to the dipole field direction are frequent in these rocks (component A), but another magnetization component, deviated from the present-day field direction (component B), can be identified in 42 sites. This component can be ante, syn or post-tilting, depending on the site, and displays normal and reversed polarities. The main results are the followings:

(1) The amount of vertical axis rotation is never large, generally smaller than about 20°.

(2) In the western and central parts of the Fars Arc, we cannot observe a coherent pattern of block rotation at the regional scale of the arc curvature. The rotations could be dominantly clockwise; most of them reflect small scale rotations associated to the movements of local strike-slip or transpressive faults. Consequently, in the western part of the Fars Arc, we cannot decide between the contradictory models of rotation predicted by Hessami *et al.* (2001a) or Talebian & Jackson (2004) on the one hand, and by Bakhtari *et al.* (1998); Molinaro *et al.* (2005); Lacombe *et al.* (2006) on the other hand. The present study underlines the existence of several mechanisms of block rotation at different scales. Further work is now in progress in the western Arc Fars in order to shed light on this question.

(3) In the Zagros-Makran syntaxis, the results are more evident. Counter-clockwise rotations are dominantly recorded in the western side of the syntaxis, while clockwise rotations are reported on the Makran side. At the scale of the syntaxis, this pattern of block rotation agrees with the rotations predicted by several authors (Molinaro *et al.* 2004; Sepehr & Cosgrove 2004). These results are also consistent with the change in orientation of the folds around the syntaxis, together with the lineation pattern of the magnetic fabric (Aubourg & Robion 2002; Aubourg *et al.* 2004) and the geodetic measurements recorded in the same area. All these observations suggest a secondary amplification of the syntaxis in a shortening fan-shaped pattern, which is in agreement with the hypothesis of the indentation of the Oman peninsula into Eurasia.

ACKNOWLEDGMENTS

The authors acknowledge the Institute of Geophysics from the University of Tehran, the Geological Survey of Iran, to have provided us with very helpful logistics. We thank M. Molinaro, S.Sherkaty, D. Frizon de Lamotte, P. Leturmy, O. Bellier, O. Lacombe, R. Bayer for valuable discussions. This work is funded by INSU-CNRS 'Intérieur de la Terre' and 'DYETI' French national program (leaded by D. Hatzfeld).

REFERENCES

Alavi, M., 1994. Tectonics of the Zagros orogenic belt of Iran: new data and interpretations, *Tectonophysics,* **229,** 211–238.

Aubourg, C. & Robion, P., 2002. Composite ferromagnetic fabrics (magnetite, greigite) measured by AMS and partial AARM in weakly strained sandstones from western Makran, *Geophys. J. Int.,* **151,** 729–737.

Aubourg, C. *et al.* (eds), 2004. Post Miocene Shortening Pictured by Magnetic Fabric Across The Zagros-Makran Syntaxis (Iran), in *Orogenic Curvatures; Integrating Paleomagnetic and Structural Analyses,* 383. Special paper – Geological Society of America, pp. 17–40.

Authemayou, C., Chardon, D., Bellier, O., Malekzadeh, Z., Shabanian, E. & Abbassi, M.R., 2006. Late Cenozoic partitioning of oblique plate convergence in the Zagros fold-and-thrust belt (Iran), *Tectonics,* **25**(3), TC3002.

Bakhtari, H., Frizon de Lamotte, D., Aubourg, C. & Hassanzadeh, J., 1998. Magnetic fabric of tertiary sandstones from the arc of Fars (Eastern Zagros, Iran), *Tectonophysics,* **284,** 299–316.

Bayer, R. *et al.*, 2006. Active deformation in Zagros-Makran transition zone inferred from GPS measurements, *Geophys. J. Int.,* **165,** 373–381.

Berberian, M., 1995. Master "blind" thrust faults hidden under the Zagros folds: active basement tectonics and surface morphotectonics, *Tectonophysics,* **241,** 193–224.

Besse, J. & Courtillot, V., 1991. Revised and synthetic apparent polar wander paths of the African, Eurasian, North American and Indian plates, and true polar wander path since 200 Ma, *J. Geophys. Res.,* **98,** 4029–4050.

Blanc, E.J.-P., Allen, M.B., Inger, S. & Hassani, H., 2003. Structural styles in the Zagros Simple Folded Zone, Iran, *J. Geol. Soc., Lond.,* **160,** 401–412.

Chauvin, A., Perroud, H. & Bazhenkov, M.L., 1996. Anomalous low paleomagnetic inclinations from Oligocene-Lower Miocene red beds of the south-west Tien Shan, central Asia, *Geophys. J. Int.,* **126**(2), 303–313.

Cogné, J.P., 2003. Paleomac: a MacintoshTM application for treating paleomagnetic data and making plate reconstruction, *Geochem. Geophys. Geosyst.,* **4**(1), 1007, doi:10:1029/2001GC000227.

Cosgrove, J.W. & Ameen, M.S., 2000. A comparison of the geometry, spatial organisation and fracture patterns associated with forced folds and buckle folds, in *Forced Folds and Fractures,* eds Cosgrove, J.W. & Ameen, M.S., Geol. Soc. Lon. Spec. Pub.

Davis, D.M. & Engelder, T., 1985. The role of salt in fold-and-thrust belts, *Tectonophysics,* **119,** 67–88.

Delaunay, S., Smith, B. & Aubourg, C., 2002. Asymmetrical fold test in the case of overfolding: two examples from the Makran accretionary prism (Southern Iran), *Phys. Chem. Earth, Parts A/B/C,* **27**(25–31), 1195–1203.

Engdahl, E.R. & Bergman, E.A., 2004. Improved locations and focal depths for well-constrained teleseismic earthquakes occuring in the Iran region (1909–2002), EGU 1st general assembly, Nice.

Fischer, R.A., 1953. Dispersion on a sphere, *Proc. Roy. Soc. Lond., Ser. A,* **217,** 295–305.

Furst, M., 1990. Strike-slip faults and diapirism of the south-eastern Zagros ranges, in *Proceedings of the Symposium on Diapirism,* Bandar Abbas, Iran, pp. 149–183.

Hessami, K., Koyi, H.A. & Talbot, C.J., 2001a. The significance of strike-slip faulting in the basement of the Zagros fold and thrust belt, *J. Petrol. Geol.,* **24**(1), 5–28.

Hessami, K., Koyi, H.A., Talbot, C.J., Tabasi, H. & Shabanian, E., 2001b. Progressive unconformities within an evolving foreland fold-thrust belt, Zagros Mountains, *J. Geol. Soc., Lond.,* **158,** 969–981.

Homke, S., Vergés, J., Garcés, M., Emami, H. & Karpuz, R., 2004. Magnetostratigraphy of Miocene-Pliocene Zagros foreland deposits in the front of the Push-e Kush Arc (Lurestan Province, Iran), *Earth planet. Sci. Lett.,* **225,** 397–410.

Jackson, J.A., Haines, J. & Holt, W., 1995. The accommodation of Arabia-Eurasia plate convergence in Iran, *J. Geophys. Res.,* **100**(b8), 15 205–15 219.

Kadinski-Cade, K. & Barazangi, M., 1982. Seismotectonics of southern Iran: the Oman line, *Tectonics,* **1**(5), 389–412.

Lacombe, O., Mouthereau, F., Kargar, S. & Meyer, B., 2006. Late Cenozoic and modern stress fields in the western Fars (Iran): implications for the tectonic and kinematic evolution of Central Zagros, *Tectonics,* **25,** TC1003.

McClay, K.R., Whitehouse, P.S., Dooley, T. & Richards, M., 2004. 3D evolution of fold and thrust belts formed by oblique convergence, *Mar. Petrol. Geol.,* **21,** 857–877.

McQuarrie, N., 2004. Crustal scale geometry of the Zagros fold-thrust belt, Iran, *J. Struct. Geol.,* **26**(3), 519–535.

Molinaro, M., Guezou, J.C., Leturmy, P., Eshraghi, S.A. & de Lamotte, D.F., 2004. The origin of changes in structural style across the Bandar Abbas syntaxis, SE Zagros (Iran), *Mar. Petrol. Geol.,* **21**(6), 735–752.

Molinaro, M., Leturmy, P., Guezou, J.-C. & Frizon de Lamotte, D., 2005. The structure and kinematics of the south-eastern Zagros fold-thrust belt; Iran: from thin-skinned to thick-skinned tectonics, *Tectonics,* **24,** TC3007.

O'Brien, C.A.E., 1957. Salt Diapirism in south Persia, *Geologie en Mijnbouw,* **19,** 357–376.

Regard, V., Bellier, O., Thomas, J.-C., Abbassi, M.R., Mercier, E., Shabanian, E., Feghi, K. & Soleymani, S., 2004. Accomodation of Arabia-Eurasia convergence in the Zagros Makran transfer zone, SE Iran : a transition between collision and subduction through a young deforming system, *Tectonics,* **23,** TC407.

Regard, V., Faccenna, C., Martinod, J. & Bellier, O., 2005. Slab pull and indentation tectonics: insights from 3D laboratory experiments, *Phys. Earth planet. Inter.,* **149,** 99–113.

Richard, P., Mocquet, B. & Cobbold, P.R., 1991. Experiments on simultaneous faulting and folding above a basement wrench fault, *Tectonophysics,* **188,** 133–141.

Ricou, L.E., 1976. Évolution structurale des Zagrides: la région clef de Neyriz (Zagros iranien), *Mem. Soc. Geol. France,* **125,** 140.

Ricou, L., Braud, J. & Brunn, J.H., 1977. Le Zagros, *Memoires Societé Geologique de France,* **8,** 33–52.

Ron, H., Freund, R., Garfunkel, Z. & Nur, A., 1984. Block rotation by strike-slip faulting: structural and paleomagnetic evidence, *J. Geophys. Res.,* **89**(B7), 6256–6270.

Sattarzadeh, Y., Cosgrove, J.W. & Vita-Finzi, C., 2002. The geometry of structures in the Zagros cover rocks and its neotectonic implications, in *The Tectonic and Climatic Evolution of the Arabian Sea Region,* eds Clift, P.D., Kroon, D., Gaedicke, C. & Craig, J., Geol. Soc. Lon. Spec. Pub., London.

Sepehr, M. & Cosgrove, J.W., 2004. Structural framework of the Zagros Fold-Thrust, Iran, *Mar. Petrol. Geol.,* **21,** 829–843.

Sherkati, S. & Letouzey, J., 2004. Variation of structural style and basin evolution in the central Zagros (Izeh Zone and Dezful Embayment, Iran), *Mar. Petrol. Geol.,* **21,** 535–554.

Smith, B., Aubourg, C., Guezou, J.-C., Nazari, H., Braud, X. & Guya, N., 2003. *Paleomagnetic investigation of a sigmoidal fold in the Zagros-Makran syntaxis (Southern Iran) and kinematic implication,* EGS-AGU-EUG joint assembly, Nice.

Smith, B., Aubourg, C., Guezou, J.-C., Nazari, H., Molinaro, M., Braud, X. & Guya, N., 2005. Kinematics of a sigmoidal fold and vertical axis rotation in the east of the Zagros–Makran syntaxis (southern Iran): Paleomagnetic, magnetic fabric and microtectonic approaches, *Tectonophysics,* **411,** 89–109.

Talebian, M. & Jackson, J., 2004. A reappraisal of earthquake focal mechanisms and active shortening in the Zagros mountains of Iran, *Geophys. J. Int.,* **156,** 506–526.

Vernant, P. *et al.*, 2003. Contemporary crustal deformation and plate kinematics in Middle East constrained by GPS measurements in Iran and northern Oman, *Geophys. J. Int.,* **157,** 381–398.

Walker, R., Jackson, J. & Baker, C., 2003. Surface expression of thrust faulting in eastern Iran; source parameters and surface deformation of the 1978 Tabas and 1968 Ferdows earthquake sequence, *Geophys. J. Int.,* **152**(3), 749–765.